EPJ Plus

EPJ.org
your physics journal

Eur. Phys. J. Plus (2018) **133**: 344 DOI 10.1140/epjp/i2018-12187-6

Influence of space charge density on electron energy distribution function and on composition of atmospheric pressure He/O_2/air plasmas

Željko Mladenović, Saša Gocić, Dragana Marić, Zoran Lj. Petrović

Società Italiana di Fisica

Springer

Eur. Phys. J. Plus (2018) **133**: 344
DOI 10.1140/epjp/i2018-12187-6

THE EUROPEAN PHYSICAL JOURNAL PLUS

Regular Article

Influence of space charge density on electron energy distribution function and on composition of atmospheric pressure He/O_2/air plasmas

Željko Mladenović[1,a], Saša Gocić[1], Dragana Marić[2], and Zoran Lj. Petrović[2,3]

[1] Department of Physics, Faculty of Sciences and Mathematics, University of Niš, Višegradska 33, 18000 Niš, Serbia
[2] Institute of Physics, University of Belgrade, Pregrevica 118, 11080 Belgrade, Serbia
[3] Serbian Academy of Sciences and Arts, Knez Mihailova 35, 11001 Belgrade, Serbia

Received: 23 April 2018 / Revised: 9 July 2018
Published online: 30 August 2018

Abstract. Atmospheric pressure non-equilibrium plasma represents an efficient source of reactive species for different kinds of applications. Rich chemistry of such plasmas develops on longer time scales and is difficult to handle by kinetic models so global models are often applied to study such processes. The Maxwell-Boltzmann (MB) distribution is often used in global modelling of these non-equilibrium systems, even for the calculation of electron rate coefficients. In order to test the sensitivity of plasma composition on the space charge density and consequently on the assumed electron energy distribution function (EEDF), the zero-dimensional global model is applied to the helium/oxygen mixture (0.5% of O_2) with humid air impurities. To test the effect of the distribution function on global models we have included the data calculated based on the non-equilibrium EEDF for the processes where often exponential Arrhenius-like formulae as a function of the effective temperature are used. The initial calculation showed that the change in the form of distribution function mainly affects the processes with thresholds considerably higher than the mean electron energy while it does not change much the rates for the processes with the thresholds and peaks of the cross sections in the region of the mean energy. We have calculated variations of the EEDF with the charge density and the resulting changes in chemical kinetics.

1 Introduction

The fast growing applications of complex plasma systems in various fields [1], such as material processing [2,3], bio-medical applications [1,4,5] and surface modification [6,7], opened the new forms of non-equilibrium plasmas that require detailed modeling and understanding of the basic phenomenology in order to optimize existing applications and open further possibilities. At atmospheric pressure chemistry is more complex, both because of higher collision rates and due to the fact that three body processes are also open. In addition, in combination with the atmospheric mixture of gases the presence of water vapour provides additional complexity due to a number of ion-molecule reactions, different possible radicals and formation of clusters. Having in mind that the chemical composition of complex plasmas is often difficult to access by measurements, studies based on numerical models play an important role in the development of new devices. Due to their complexity atmospheric pressure plasmas are particularly difficult to describe by models. The most frequently used method of producing atmospheric pressure non-equilibrium plasma is to start a discharge in a flow of helium, pure or in a mixture with oxygen. Furthermore the plasma is mixed with the external air, humid air or applied to the liquid. Recently such plasmas have been represented by models of discharges in helium mixtures with oxygen [8], water [9,10], humid or real air [11,12], or in mixture with oxygen and water or humid-air [13–15]. In a recent paper [16] plasma interactions with liquid water were reviewed.

Results of zero-dimensional (0D) global models used for investigation of influence of humid air on chemistry of reactive species in rf-driven atmospheric-pressure (AP) helium-oxygen mixture (0.5% of O_2) plasmas were presented in a number of recent papers [14,15,17]. We chose to use the set of data from [15,17] and other related papers from the same group of authors in order to test our code. This model was chosen above all things as it was well documented

[a] e-mail: zeljkom@pmf.ni.ac.rs

and it comprises a reaction scheme with 1048 reactions for the kinetics of 59 species. The second goal was trying to compare how the choice of electron energy distribution function affects the kinetics of species in such plasmas so we did not venture into updating any of the rates in the model.

Typically, in global models two types of rate coefficients are used. The first group is calculated from the Boltzmann equation (BE), *i.e.* it represents the non-equilibrium distribution function. The parameter for such calculations is the effective electric field E/N (or the corresponding mean energy). In the second group coefficients are provided in a form of exponential dependence for the rates, resembling Arrhenius formula, or in other words equilibrium processes for a given temperature. The condition for TE (or LTE) is that the external vessel is also at the fixed temperature and is driving the system. This requirement is often overlooked. In plasmas we have boundaries that are at some lower temperature and are unable to provide the energy to drive the system. Thus even when EEDFs are Maxwellianized one has double temperature EEDF or EEDFs even much more complex than that due to energy losses at surfaces. The two rates MB and BE may be different by several orders of magnitude even for the same mean energy, as has been illustrated in a number of papers [18,19]. The difference is in the fact that systems in thermodynamic equilibrium (as described by the Maxwell-Boltzmann distribution function-MB) have an input of energy from the boundaries of the vessels *i.e.* the entire system is maintained at a fixed temperature. On the other hand, the systems in non-equilibrium (as described by the solution to the Boltzmann equation-BE) have to balance gains from the field with the losses and that balancing equilibration may be non-local. In that case the effect of the walls which are at room temperature is unimportant. Thus, typically (but not necessarily) the MB rates are very large at high energies while BE results show depletion due to losses through electronic excitation and ionization. Often global models are realized with BE results being used for electrons and MB for ions (assuming that ions are at room temperature) which seems reasonable for the bulk of the plasma but not so much for the sheaths and double layers. In many cases, even for electrons, due to the lack of cross section data some of the BE results are replaced by MB based formulae for some specific temperatures used to fit different experimental data. While effective for a narrow range of energies such approximation is clearly invalid in a broad energy range. The idea of this paper is to illustrate differences that may occur in the composition of a plasma when both MB and BE data are available.

In addition, we have added a parametric study considering the degree of ionization through its effect on the EEDF. This is calculated by taking advantage of a facility in the BOLSIG+ [20] code that we are using. More details about the calculating procedure and the influences of Coulomb collisions on the EEDF were given recently [20,21]. Otherwise making calculations of the EEDF under conditions where space charge affects the EEDF would be quite difficult [22]. We have performed calculations for our set of conditions, however, conclusions are general and broadly applicable.

The term global model has been assumed mainly to represent zero-dimensional models that are aimed at following very detailed chemical kinetics. These limitations have been challenged in the meantime, for example energy balance was solved with spatial resolution in order to produce the profile of particles especially the shorter lived species and also overall integral production rates of the longer lived products [23,24]. Most importantly the production of active species in a global model needs to be represented by some connections to the energy distribution function (most importantly the electron energy distribution function) either local or global. On the other hand, some of the main advantages of the global model are: a large number of participating reactants and even a much greater number of reactions; a large gap in time scales between chemical processes and establishment of relaxed densities of different molecules and kinetics of electrons and ions; a large dynamic range in densities of different species, whereby their numbers may be too small to observe their activity by standard sampling techniques.

At the same time other models, fluid in particular, have the same strategy of connecting to chemical reactions and even more critically to the transport coefficients needed to solve the fluid equations for the flow of charges and their spatial profiles. In those models it is customary to use swarm data either measured or calculated from the Boltzmann equation in the form of lookup tables [3,11,25,26]. The treatment of non-local kinetics in sheaths has opened the need to introduce additional sets of data for high energy particles separately from the data for the mean energy. The simplest technique was the introduction of the relaxation continuum model [27], and later on an introduction of hybrid models [28,29] or even fully kinetic models such as the PIC MCC (Particle in cell Monte Carlo Collision) models [30]. For the purpose of the streamer discharge modeling, high order fluid models were developed which primarily emphasizes the importance of involving energy flux equations for the correct description of streamer dynamics [31,32]. These models provide spatial profiles of mean energy, high energy tails and also of fully developed distribution functions required to represent independently higher energies and mean energies of electrons (and other particles). Thus, kinetic codes do not suffer from limitations due to the use of a Maxwellian distribution function associated with the mean electron energy.

Several low-order chemical kinetics models have been developed to test the effect of excited species on the transport properties in a self-consistent manner. Those have been used in particular to follow non-equilibrium vibrational state population kinetics [33–36], kinetics of electrons under the influence of metastable population (in rare gases for example) [37–39] or the effect of radicals on transport data [40]. These models may be regarded as swarm models or global models [41] and in principle could be grouped together with the standard global models as they indicate the strategy of using the input data and representing plasma through the mean energy of electrons. Under those circumstances it has been clearly shown that rates of processes with higher thresholds (energy or particle losses/gains) cannot be represented well by a Maxwellian associated with mean energy [18,19].

At the same time, global models are often employed when one needs to establish complex kinetics involving a large number of species including those whose generation does not impart heavy losses on the energy balance. Under those circumstances it is often necessary to use from the literature the entire sets of collisional rates and probabilities that often include Arrhenius-like formulae based on a Maxwellian distribution. The choice of energy for those formulae is often an issue but always it is related to the mean energy rather than the high-energy tail.

Energy is often just established from the previous modeling papers, taken as a parameter or from Langmuir Probe measurements [42]. It is questionable whether Langmuir probe measurements using two temperatures can represent the high-energy tail of the EEDF very well. However, even in global models comparisons of Boltzmann equation solutions and Maxwell distribution based formulae have been made but in different conditions. For the low pressures Meeks and Shon [43] made a comparison of model results using Maxwellian EEDFs, as well as reaction-rate coefficients determined as a function of average electron energy through the solution of the Boltzmann equation, for chlorine chemistry. The authors concluded that the Maxwellian EEDF results in higher ionization rates and lower electronegativity compared to the calculation based on using the Boltzmann equation to determine EEDFs. On the other hand, the authors claimed that the predicted trends with power, pressure, and flow rate are similar for the two distributions and that the difference between predicted electron densities may be within quantitative measurement capabilities. More explicit conclusions were made for global models by Gudmunsson [44] but for comparison between the Maxwellian and what the author labels as the Druyvesteyn distribution. One should bear in mind that the Druyvesteyn distribution is a special case for a simplified set of cross sections and that for all gases EEDFs are much more complex. Similar conclusions were reached for higher pressures [45–47].

On the other hand, there are still numerous papers where MB rates are used in global modeling of non-equilibrium plasmas perhaps as a consequence of the lack of information from primary references for those rates [15,48–50] which was the primary motivation for our work with a specific caveat that this work pertains to atmospheric pressure plasma jets and to global models only. Some state-of-the-art global codes have the Boltzmann solver as the integral part and do not suffer from the issues discussed here (although one could argue that for thermal plasmas Maxwellian formulae could have an advantage). One such example is the GlobalKin program [51,52].

Another issue that has not been addressed under those circumstances is the fact that for some values of E/N (mean energies) the Boltzmann solution may be higher than the Maxwellian high energy tail [19] or in other words the Boltzmann solution may provide higher rates than the Maxwellian.

Having said in detail about the inadequacy of using a Maxwellian distribution one should also bear in mind that for plasmas with somewhat higher charge densities, the EEDF becomes more Maxwell-like (although the high-energy tail is still difficult to establish) and may be a better approximation than the fully non-equilibrium Boltzmann equation solution in the zero space charge limit. It is important to establish which conditions are pertinent to the plasma being modeled.

It has recently been attempted to start a wide range of benchmarking verifications of the codes [53] and chemical rate data sets [54]. Our paper was aimed at establishing the initial benchmarking starting point in a attempt to enrich the data set and test various contributions and kinetics of several key species. Having the limitations and advantages of global models in mind we have set out to give an indication of just how this connection to the energy distribution function should be developed. This is done in relation to the very frequent application of global models in the modeling of atmospheric pressure plasma jets [8,11,15]. Such plasmas offer rich chemical activity with helium as the buffer gas, atmospheric gases and water vapour in varying compositions. In addition to the complex chemistry developed on a larger spatial scale and temporal scale, the passage of ionization fronts that is a streamer-like discharge involves a high-density front with charge separation and very high field and high gradient, background discharge with low field but still significant mean energy that is driving the overall chemistry and also involves boundary effects (both radially and axially). In light of the application of these discharges in plasma medicine [1,5] and agriculture [55] one needs to follow the kinetics of specific reactive species that may not be significant players in the overall plasma kinetics or in other words one needs very detailed models with a large number of reactions and species. Such models are often too complex to include within fluid or kinetic models and need to be developed separately.

This paper is thus focused on establishing the benchmark calculations for our further studies and inclusion of more processes as well as for the general use of the cross sections and Boltzmann equations whenever possible within the framework of modeling atmospheric pressure plasma jets and related discharges. These issues have been dealt with previously within the context of more complex codes, coupled swarm and chemistry codes, often at lower pressures and often in a different set of constituent gases.

We have created a numerical code for solving a system of nonlinear, time-dependent rate equations of a zero-dimensional global model with an idea to test sensitivity of plasma composition to the selected EEDF. In doing so, we start from the chemical scheme in appendix [15]. Rate coefficients for electron molecule collisions are first used as the function of electron temperature, with an assumption of MB EEDF as is done in paper [15], and then calculated with the non-equilibrium EEDF, by using the two-term approximation BE solver BOLSIG+. MB rate coefficients are also crosschecked against online MB calculations [56]. Furthermore, we have made the estimation of a relative (percentage) contribution of each reaction from the scheme in appendix [15] and have established the main chemical processes in the creation and destruction of important plasma species.

Table 1. List of plasma species included in the global model.

	Reactive species	He^*, $He_2{}^*$, O, $O(^1D)$, $O(^1S)$, $O_2(v=1)$, $O_2(v=2)$, $O_2(v=3)$, $O_2(v=4)$, $O_2(^1\Delta)$, $O_2(^1\Sigma)$, O_3, CO_3, CO_4, N, $N(^2D)$, $N(^2P)$, $N_2(v=1)$, $N_2(v=2)$, $N_2(v=3)$, $N_2(v=4)$, NO_3, H, OH
Ions	Positive ions	He^+, $He_2{}^+$, O^+, $O_2{}^+$, $O_4{}^+$, N^+, $N_2{}^+$, $N_4{}^+$, NO^+, H_2O^+, H_3O^+
	Positive ion clusters	$O_2{}^+ \cdot H_2O$, $H_3O^+ \cdot H_2O$, $H_3O^+ \cdot OH$
	Negative ions	O^-, $O_2{}^-$, $O_3{}^-$, $O_4{}^-$, NO^-, $NO_2{}^-$, $NO_3{}^-$, $CO_3{}^-$, $CO_4{}^-$
	Negative ion clusters	$O_2{}^- \cdot H_2O$, $NO_2{}^- \cdot H_2O$, $NO_3{}^- \cdot H_2O$, $CO_3{}^- \cdot H_2O$, $CO_4{}^- \cdot H_2O$

2 Model

The governing nonlinear differential rate equations in a 0D global model can be expressed as follows:

$$\frac{\mathrm{d}n_i}{\mathrm{d}t} = \sum_j \sum_m k_{jm}^{(C)} n_j n_m + \sum_l \sum_p \sum_q k_{lpq}^{(C)} n_l n_p n_q - n_i \sum_r k_{ir}^{(D)} n_r - n_i \sum_s \sum_f k_{isf}^{(D)} n_s n_f, \tag{1}$$

where t, n_i, $n_j, \ldots, n_f$ denote time, number density of i-th, j-th, ..., and f-th species, $k_{jm}^{(C)}$ denote the two-body reaction rate coefficient for j-th and m-th species, $k_{lpq}^{(C)}$ denote three-body reaction rate coefficient for l-th, p-th and q-th species, $k_{ir}^{(D)}$ denote two-body reaction rate coefficient for i-th and r-th species and $k_{isf}^{(D)}$ denote three-body reaction rate coefficient for i-th, s-th and f-th species, respectively. Superscripts "(C)" and "(D)" denote the rate coefficient for i-th species creation and destruction, respectively. Numerous global models [24], including the present work, are made for a uniform infinite system by using the mean energy as a parameter connecting different sources of input data. In some cases, however, the energy balance is calculated [23] and some allowances are made for spatially dependent (non-local) mean energy and sources of electrons.

The reaction scheme, adopted from paper [15], comprises 1048 reactions among 59 species: neutral species, vibrationally excited species and metastables, positive and negative atomic and molecular ions and various hydrate cluster ions, as shown in table 1 for the sake of clarity. The initial plasma composition in the global model is taken as He+0.5% O_2 + 250 ppm of humid air (78% N_2, 21% O_2, 10^{-2}% CO_2, 10^{-3}% N_2O, 10^{-5}% NO_2, 10^{-6}% NO), with 1% of relative humidity (*i.e.* the same as in paper [15]).

Two-body rate coefficients for electron impact processes are calculated as [3]

$$k_{i,exc} = \sqrt{2/m_e} \int_{\varepsilon_{thr}}^{\infty} Q(\varepsilon) \sqrt{\varepsilon} f(\varepsilon) \mathrm{d}\varepsilon, \tag{2}$$

where m_e, ε, $Q(\varepsilon)$ and $f(\varepsilon)$ denote electron mass, energy, appropriate total cross section and EEDF, respectively. If the Maxwell-Boltzmann distribution is assumed, the rate coefficients can be expressed as a parametric function of electron temperature T_e in [eV] (mean electron energy), in an extended Arrhenius form,

$$k_{i,exc}(T_e) = A T_e^B \exp(-C/T_e), \tag{3}$$

where A, B and C are numerical constants, which could be determined from eq. (2) for a given set of cross sections. The list of electron-impact processes, with rate coefficients in the form (3) taken from papers [15,17], is presented in table 2.

Table 2. List of selected electron-impact processes and rate coefficients as a function of T_e [eV], taken from papers [15,17]. Units: Two-body rate coefficient [cm^3/s]. Three-body rate coefficient [cm^6/s]. Electron temperature T_e [eV]. Normalized gas temperature $T_0 = T_g$ [K]/300 K. Gas temperature $T_g = 345$ K as in paper [15].

R.N.	Reaction	Rate coefficient
R1	$He + e^- \rightarrow He^* + e^-$	$4.2 \cdot 10^{-9}\, T_e^{0.31} \exp(-19.8/T_e)$
R2	$He + e^- \rightarrow He^+ + 2e^-$	$1.5 \cdot 10^{-9}\, T_e^{0.68} \exp(-24.6/T_e)$
R3	$O_2 + e^- \rightarrow {O_2}^+ + 2e^-$	$9.0 \cdot 10^{-10}\, T_e^{2.0} \exp(-12.6/T_e)$
R4	$O_2 + e^- \rightarrow O_2(^1\Delta) + e^-$	$1.37 \cdot 10^{-9} \exp(-2.14/T_e)$
R5	$O_2 + e^- \rightarrow O_2(^1\Sigma) + e^-$	$3.24 \cdot 10^{-10} \exp(-2.218/T_e)$
R6	$N_2 + e^- \rightarrow N + N + e^-$	$1.0 \cdot 10^{-8}\, T_e^{0.5} \exp(-16.0/T_e)$
R7	$N_2 + e^- \rightarrow {N_2}^+ + 2e^-$	$1.1 \cdot 10^{-8}\, T_e^{0.5} \exp(-17.2/T_e)$
R8	$H_2O + e^- \rightarrow H + OH + e^-$	$1.8 \cdot 10^{-10}$
R9	$O_2(^1\Sigma) + e^- \rightarrow {O_2}^+ + 2e^-$	$2.34 \cdot 10^{-9}\, T_e^{1.03} \exp(-10.663/T_e)$
R10	$O_2(^1\Delta) + e^- \rightarrow {O_2}^+ + 2e^-$	$2.34 \cdot 10^{-9}\, T_e^{1.03} \exp(-11.31/T_e)$
R11	$O + e^- \rightarrow O^+ + 2e^-$	$9.0 \cdot 10^{-9}\, T_e^{0.7} \exp(-13.6/T_e)$
R12	$N + e^- \rightarrow N^+ + 2e^-$	$1.0 \cdot 10^{-8}\, T_e^{0.5} \exp(-14.5/T_e)$
R13	$O_2 + e^- \rightarrow O + O^-$	$1.07 \cdot 10^{-9}\, T_e^{-1.39} \exp(-6.26/T_e)$
R14	$O_2(^1\Sigma) + e^- \rightarrow O + O^-$	$4.19 \cdot 10^{-9}\, T_e^{-1.376} \exp(-4.54/T_e)$
R15	$O_2(^1\Delta) + e^- \rightarrow O + O^-$	$4.19 \cdot 10^{-9}\, T_e^{-1.376} \exp(-5.19/T_e)$
R16	$O_2 + e^- + M \rightarrow {O_2}^- + M$	$3.6 \cdot 10^{-31}\, T_e^{-0.5}$ for M = He, O_2
		$1.24 \cdot 10^{-31}\, T_0^{-0.5}$ for M = N_2
		$3.9 \cdot 10^{-35}$ for M = $O_2(^1\Delta)$
		$1.0 \cdot 10^{-31}$ for M = O
		$1.4 \cdot 10^{-29}$ for M = H_2O

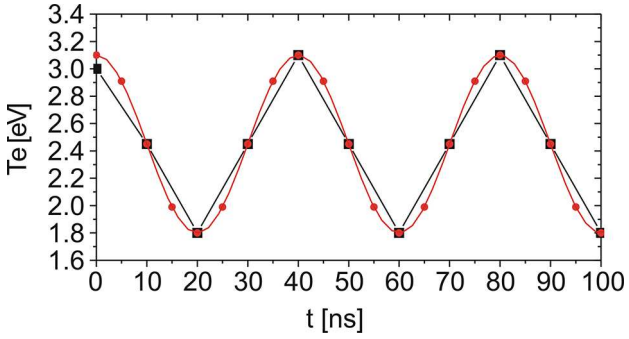

Fig. 1. Sinusoidal fit for electron temperature (line and circles) and triangular form (line and squares) from paper [15].

These processes have been selected for testing the influence of EEDF and these rate coefficients will also be calculated under the assumption of a non-equilibrium EEDF for the E/N resulting in the same mean energy.

The system of rate equations is solved by MATLAB ODE15s solver, with relative and absolute tolerances equal to 10^{-12} and 10^{-6}, respectively. A similar modeling procedure was applied in the case of a surface micro-discharge in humid air at atmospheric pressure [14], up to 1000 s. In our model, the pulse duration of 5 ms with the time-step of 10 ns and electron concentration fixed at the value of 10^{11} cm^{-3} are chosen, according to the global model results [15]. The time dependence of T_e necessary for the calculation of rate coefficients is obtained by fitting data [15] presented in fig. 1, within the interval 1.8 eV–3.1 eV, and it is given in the form

$$T_e = 0.65 \cos(2 \cdot 2\pi\nu t) + 2.45\,[\text{eV}], \quad \text{with } \nu = 12.5\,\text{MHz}. \tag{4}$$

The time dependence of T_e was chosen to be the same as given by the results [57] of one-dimensional numerical simulation of the discharge gap of a micro-scale rf-driven atmospheric plasma jet (μ-APPJ) [57] and was used for both MB and BE calculations.

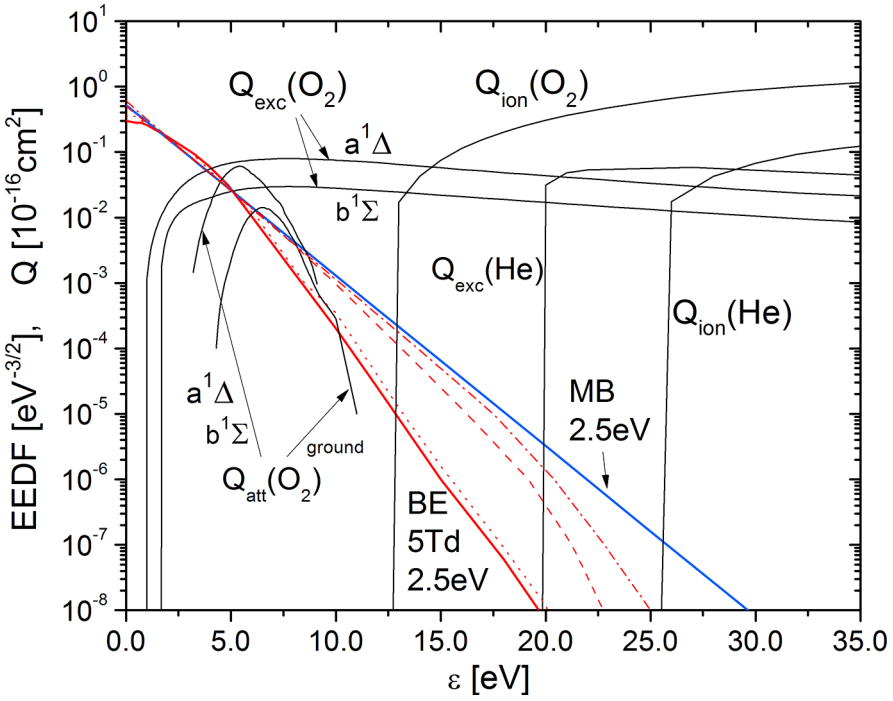

Fig. 2. Cross sections for O_2 excitation, ionization and two-body attachment, He excitation and ionization. EEDF calculated for $n_e = 10^{11}\,\mathrm{cm}^{-3}$: Maxwell-Boltzmann (MB-blue solid line) and Boltzmann equation (BE-red solid line). BE for: $n_e = 10^{15}\,\mathrm{cm}^{-3}$ —dotted red line; $n_e = 10^{17}\,\mathrm{cm}^{-3}$ —dashed red line; $n_e = 10^{19}\,\mathrm{cm}^{-3}$ —dash-dotted red line (2.5 eV mean energy). The BE result is obtained for the mixture of ≅ 99.5% He + 0.5% O_2 + 195 ppm N_2 + 2.5 ppm H_2O + 988.5 ppm O + 0.8 ppm N + 9.885 ppm $O_2(^1\Sigma)$ + 494.2 ppm $O_2(^1\Delta)$.

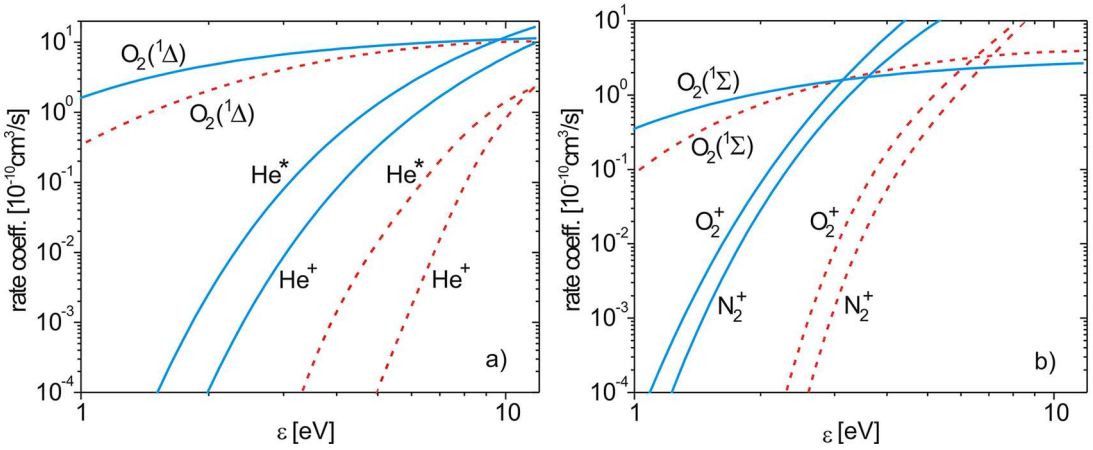

Fig. 3. Rate coefficients for: (a) O_2 excitation in $O_2(^1\Delta)$ and He excitation and ionization; (b) O_2 excitation in $O_2(^1\Sigma)$, and O_2 and N_2 ionization, based on MB (solid line) and BE (dashed line) EEDF for electron concentration $10^{11}\,\mathrm{cm}^{-3}$.

2.1 Input data

In the non-equilibrium case, rate coefficients for processes in table 2 are obtained by solving the Boltzmann equation by BOLSIG+ solver. Cross section data from the MORGAN database [58] for He, O_2, N_2 and H_2O are used as an input. Characteristic cross sections for O_2 excitation, two-body attachment, ionization, He excitation and ionization, MB and BE distributions for the same mean energy of 2.5 eV (the same effective electron temperature) are shown in fig. 2. Initial calculations are made for the mixture of He ≅ 99.5%, O_2 0.5%, N_2 195 ppm and H_2O 2.5 ppm. Furthermore, in order to compare MB and BE rate coefficients for ionizations R9, R10, R11, R12 and attachments R14, R15 from table 2, four more species are added in the previous mixture O 988.5 ppm, N 0.8 ppm, $O_2(^1\Sigma)$ 9.885 ppm and $O_2(^1\Delta)$ 494.2 ppm, obtained from plasma composition after 1 ms. The comparison between rate coefficients obtained by BOLSIG+ and the ones from table 2, is given in figs. 3(a), (b) and 4(a), (b).

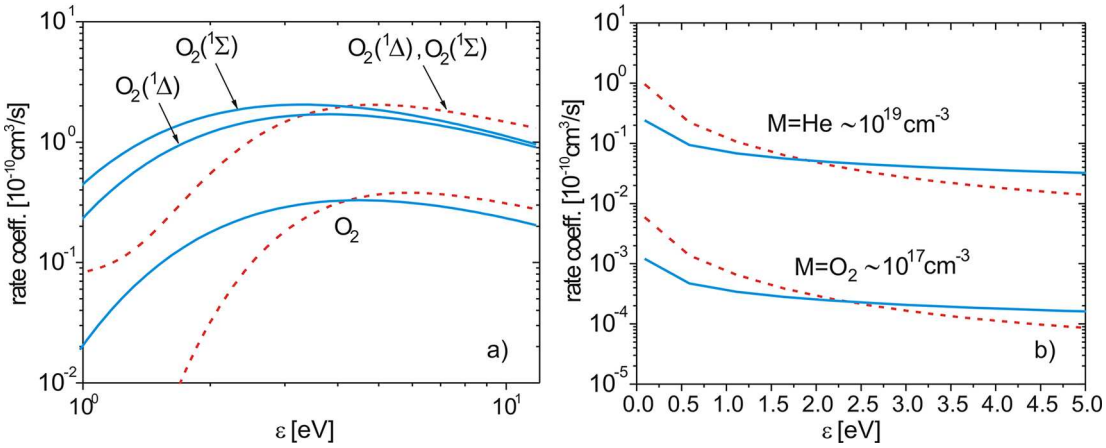

Fig. 4. Rate coefficients for: (a) 2-body attachment to O_2, and to $O_2(^1\Delta)$ and $O_2(^1\Sigma)$ states; (b) 3-body attachment with He and O_2 as the third particle, multiplied by the third particle concentration —based on MB (solid line) and BE (dashed line) EEDF for electron concentration 10^{11} cm^{-3}.

As shown in fig. 2, the BE distribution has a significantly lower high-energy tail and only a minor overlap with helium inelastic cross sections and in particular (and most importantly) with the ionization cross sections. As a consequence, the rate coefficients for He ionization and excitation (and all processes with high threshold where the differences between MB and BE are the greatest) are reduced by several orders of magnitude (fig. 3(a)). Figure 2 also shows a change of the EEDF due to the effect of charged particle collisions. The first departure from the low-charge density limit EEDF is observable at 10^{15} cm^{-3}. It begins to resemble a Maxwellian by becoming closer to a straight line in a logarithmic scale for densities above 10^{19} cm^{-3}. Still, however for a wide range of charge densities the basic non-equilibrium distribution function (unaffected by the space charge) is a good approximation. Here we assume that conditions are so adjusted that the mean electron energy is kept constant (in this calculation we have kept a constant electric field corresponding to the mean energy of 2.45 eV). The EEDF calculated for electron density 10^{17} cm^{-3} and 10^{19} cm^{-3} in fig. 2 serve to show the process of Maxwellization of the EEDF through *e*-*e* collisions. The electron density up to 10^{14} cm^{-3} was reported for low-temperature atmospheric pressure plasma jets [16]. In general, plasmas with higher densities bordering on the upper limit used here are quite different in nature, thermal, with a large degree of dissociation, ionization and with quite different composition. In particular for electron density of 10^{19} cm^{-3} one would have to make a more complex model of the energy distribution taking into account interactions between all charged particles, loading and spatial profile of the plasma. Thus the EEDF for 10^{19} cm^{-3} serves merely as an indication of how far one has to go to turn the EEDF to a Maxwellian and even than the Maxwellianization of the EEDF is not complete and we have not included the data for kinetics of various molecules, atoms and ions for this density.

One should bear in mind that we have used MB EEDF based rates only for the processes where those have been used in the recent literature. For all processes where cross sections data base is used to calculate rates using the non-equilibrium EEDF we maintain the same procedure. Even in such a limited range ofapplications of the MB EEDF differences are significant and we try to point out what these differences mean. In addition we have chosen to keep the basic background mixture as fixed (which perhaps may be applicable to the propagating plasma jet where perturbation of the plasma on the gas composition is limited) in order to represent the effect of different distribution functions.

Superelastic electron collisions can modify the BE EEDF, creating characteristic plateaux in high energy tail, caused by electronic metastable states [59] or in the lower-energy part, caused by vibrationally excited molecular N_2 or O_2 [60,61]. The EEDF presented in fig. 2 was calculated without a self-consistent calculation of the densities of excited states as following two different effects that may provide similar changes in kinetics would blur the importance of our primary target. We have only included superelastic collisions with rotational levels of the molecular components for populations at room temperature.

Furthermore, the influence of superelastic vibrational and electronic states on the EEDF can be appreciable in the afterglow (post discharge regime $E/N = 0$). Under such conditions, rate coefficients obtained by the EEDF, especially for high threshold processes, depend on the discharge conditions, *i.e.* ionization degree and concentration of excited species [62], and thus cannot be taken only as a function of average electron energy (electron temperature) in making global models. In addition, different kinetic phenomena may develop due to different non-hydrodynamic conditions [41] that may affect strongly the EEDF during the afterglow.

In the energy region around 1 eV to 3 eV, BE has a similar shape and magnitude as the MB distribution. Hence, rate coefficients for O_2 excitation are only slightly affected by the difference in the chosen EEDF (fig. 3(a)) since the threshold for the singlet delta state is around 1 eV. A similar conclusion can be made for two-body electron attachment to ground and to electronically excited O_2 molecular states (fig. 4(a)). In this case differences are slightly higher than in

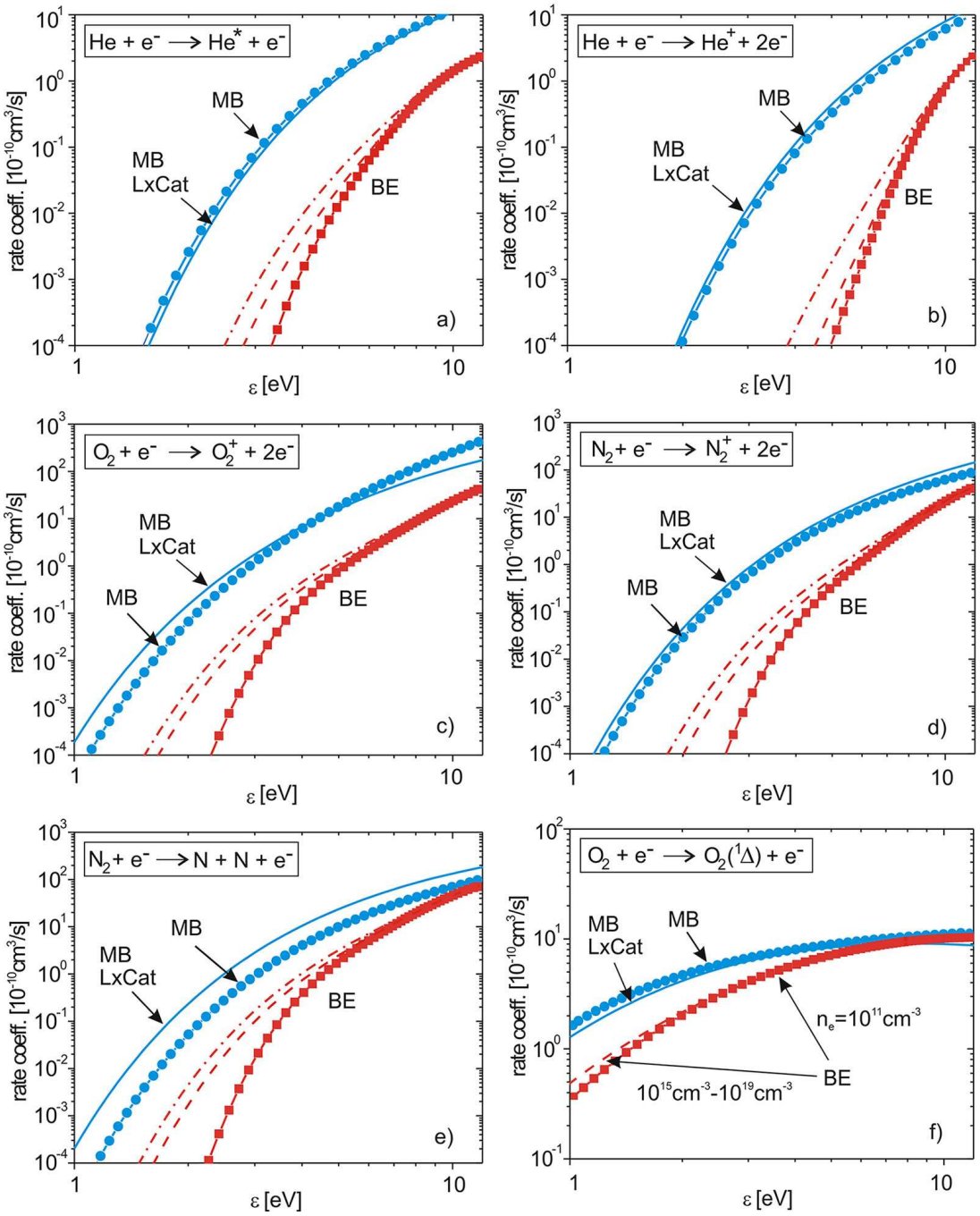

Fig. 5. Comparison of rate coefficients given in Arrhenius form (MB-blue line with circle) and rate coefficients obtained by BOLSIG+ (for $n_e = 10^{11}\,\mathrm{cm}^{-3}$: MB LxCat-blue line, BE-red line with squares; for $n_e = 10^{17}\,\mathrm{cm}^{-3}$ —dashed red line; $n_e = 10^{19}\,\mathrm{cm}^{-3}$ —dash-dotted red line) for: (a) He excitation; (b) He ionization; (c) O_2 ionization; (d) N_2 ionization; (e) N_2 dissociation; (f) O_2 excitation.

the case of the O_2 excitation, since narrow attachment cross sections reach their maximum for mean electron energies over 5 eV (fig. 2). Rate coefficients for three-body electron attachment to O_2 in fig. 4(b) are presented in the form of the two-body processes, calculated by multiplying with the concentration of the third body. For the case of Ar plasmas, the influence of the EEDF shape on the rate coefficients is illustrated in paper [18].

The comparison of MB (from table 2), BE rate coefficients for different charge densities and the rate coefficients calculated by BOLSIG+ with an assumed MB distribution (denoted as MBLxCat) [56] is presented in figs. 5(a)–(f). Online calculation for MBLxCat was made for the same plasma composition as for BE, with the same cross section data. It can be seen that BOLSIG+ for the MB EEDF gives rate coefficients comparable with those used in

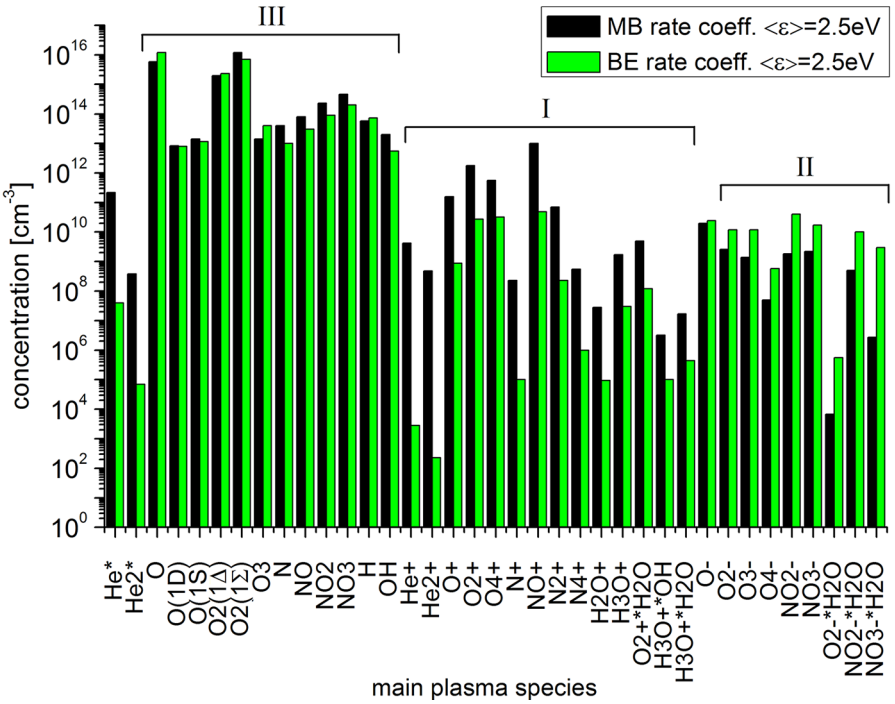

Fig. 6. The comparison of plasma composition based on MB (black bars) and BE rate coefficients (green bars), for electron density $10^{11}\,\mathrm{cm}^{-3}$. Three groups of species can be distinguished with BE rates: I —species with density that decreases; II —species with increasing density; III —species with density only slightly affected by the inclusion of the BE based rates instead of the MB based rates.

papers [15,17] so one can only assume that the same or very similar cross sections have been used to obtain those data. For processes with low energy threshold (for example O_2 excitation) there is a similarity between Arrhenius, MBLxCat and BE rate coefficients (figs. 5(a)–(f)), as to be expected according to similarity between MB and BE EEDF in the O_2 excitation energy threshold region (see fig. 2).

3 Results and discussion

3.1 Plasma composition

The comparison of plasma composition based on the results of global model calculations with the assumed MB and BE distributions is shown in fig. 6. Both sets of results are obtained for electron concentration of $10^{11}\,\mathrm{cm}^{-3}$. According to their response to change of the EEDF, we have divided the plasma species into three groups. In the first group there are helium metastable states and helium, oxygen, nitrogen and water positive ions and their water clusters, which have significantly lower concentrations in case of BE rates. The concentration of He^+ ions is reduced by several orders of magnitude, as a direct consequence of the reduced ionization coefficient shown in fig. 3(a). A similar effect on helium metastable He^* concentration is the lowering of the corresponding excitation rate coefficient in the case of BE EEDF (fig. 3(a)). The decreasing of concentrations of other positive ions will be analyzed in light of the main processes of their creation and destruction.

The second group of plasma species consists of negative ions and their water clusters, with higher concentrations in case of BE rates. Their behavior is partially a consequence of the lower positive ion concentrations, since some of the destruction channels for negative ions go through reactions with positive ions. Finally, the concentrations of neutral species and radicals in the third group are only slightly affected by choosing BE distribution, as can be seen in the case of molecular oxygen excited states $O_2(^1\Delta)$ and $O_2(^1\Sigma)$, in agreement with rate coefficient behavior in figs. 3(a), (b).

In order to put more light on reaction pathways and the underlying mechanisms leading to the observed behavior in fig. 6, in the next section we will analyze and quantify (in percentage of contribution) the main generation and loss mechanisms for the main plasma species presented on the x-axis in fig. 6. This analysis can serve as a guidance for the optimization of mixture composition (through changing the oxygen and humid air content in helium plasmas) with a presumed goal to increase the abundance of oxygen and nitrogen reactive species.

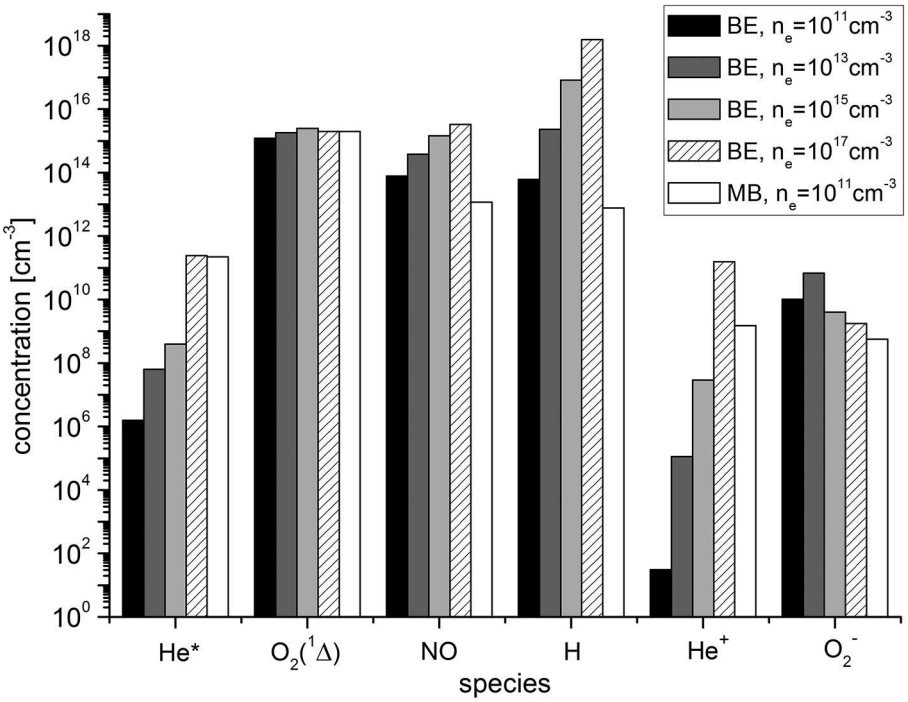

Fig. 7. Influence of charge densities on plasma compositions. The chemical composition calculated with MB and BE rate coefficients for different electron densities is marked as shown in the upper box in the figure.

3.2 The effect of the changing density of charges on plasma chemistry through its effect on the distribution function

The effect of increasing space charge on the EEDF is evident from our previous figures (figs. 2 and 5) where we compare MB and BE obtained rates for electron molecule scattering. Thus, electron-induced processes, especially dissociative processes, attachment and ionization are at the core of the resulting chemistry effects of EEDF on the final densities of most particles.

We have used a facility in BOLSIG+ code to calculate the EEDF with an increased density of charged particles. In principle this will describe only the change of the EEDF due to the effect of charged particle collisions. Here we assume that conditions are so adjusted that the mean electron energy is kept constant (in this calculation we have kept a constant electric field corresponding to the mean energy of 2.45 eV).

In figs. 5(a)–(f) we show the dependence of the rates for ionization and excitation of several states of He, O_2 and N_2 as a function of the assumed space charge density. The field was adjusted to have the same mean electron energy (T_e) as space charge changes. We can see that a significant effect on the rates is observed above $10^{15}\,cm^{-3}$. The processes peaking at low energies are not affected while there is a great effect on the processes with high thresholds.

Finally we have performed a global model for these conditions and changes in densities of several species are shown in fig. 7. There are three different behaviors in the kinetics as indicated in fig. 7. In one group, the densities increase proportionally to the increase of the electron density and sometimes they increase even faster. The proportional increase is due to the increased electron density, the faster proportional increase is due to the effects of electron density on the EEDF whereby the high energy tail increases and thus overall rate coefficients increase as well. Examples for these two possibilities are He^* and He^+. The same is true for excited states of oxygen, O^+ and $O_2{}^+$. In all those cases losses are mainly due to the molecules present in the mixture in the ground state such as He, O_2.

If the dominant losses are due to particles that are formed in reactions those particles may increase in number with electron density and thus may skew the balance of production and losses. Then one may expect the growth of a specific radical to be slower than the growth of electrons or even almost constant. The creation of NO is determined by atomic oxygen O and excited $N(^2D)$, which are dominantly created in the dissociative recombination of NO^+ ions with electrons. At higher electron densities losses due to collisions with singlet nitrogen atoms begin to dominate. The density of metastable $O_2(^1\Delta)$ is not sensitive on electron density growth since the process of electron-impact excitation of O_2 is efficiently compensated by $O_2(^1\Delta)$ quenching by $O(^1S)$. The main production of $O(^1S)$ goes through e-impact excitation of atomic O.

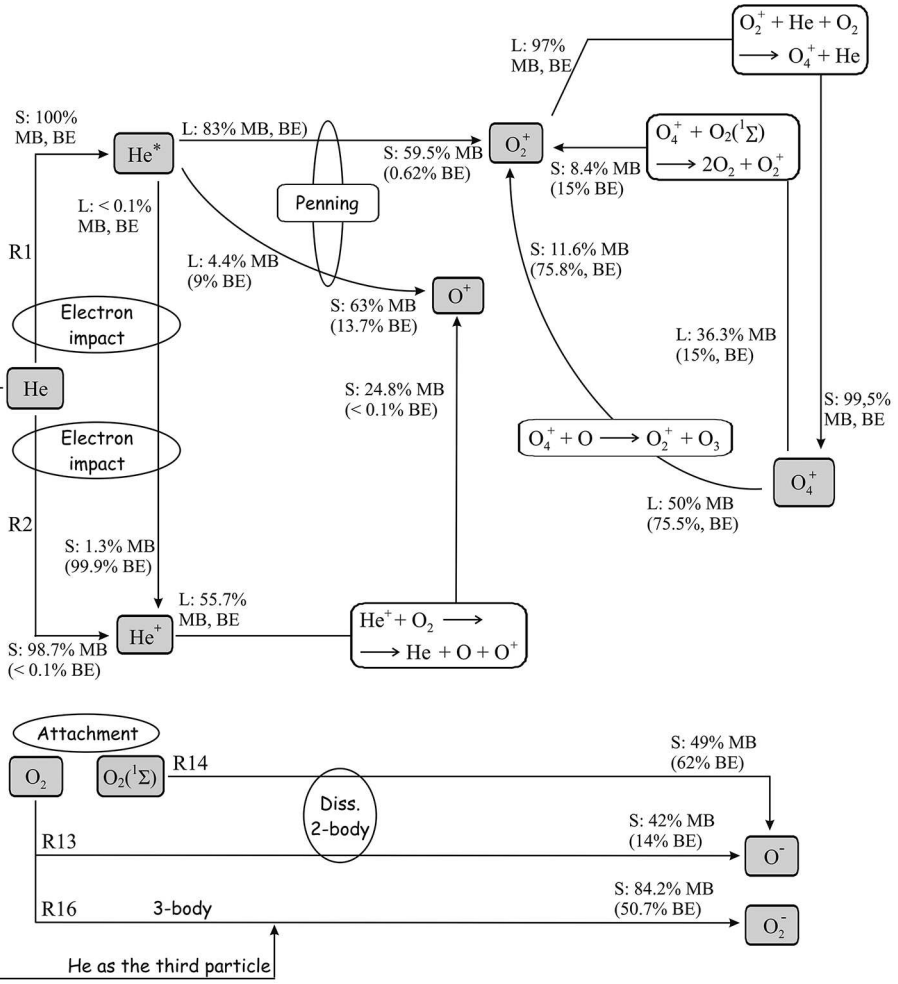

Fig. 8. The chemical pathways of generation and loss for He^*, He^+, and positive and negative oxygen ions. "S" and "L" denote the source and loss terms for individual species.

Finally as in the case of $O_2{}^-$ the main losses switch from detachment to ion-ion recombination. In the case of $O_2{}^-$ important destruction mechanisms involve O^+, $O_2{}^+$, $O_4{}^+$ and NO^+ ions. As a result of all those processes density first increases and then decreases as the recombination becomes more efficient.

In addition, we have made calculations of kinetics where electron density changes only affected the EEDF but the actual electron density in the gas was maintained at $10^{11}\,\mathrm{cm}^{-3}$. There were only species that increased in density proportionally to the electron density or even faster and there were also species that did not change almost at all in the density as their threshold energy was in the region of low energies and thus not affected by electron density.

3.3 The main physicochemical processes and reaction pathways

In order to quantify the influence of the assumed EEDF on the chemical kinetics of a particular plasma species we have calculated the percentage of contribution for all processes on the right-hand side in eq. (1). The results presented in this section are for the electron concentration of $10^{11}\,\mathrm{cm}^{-3}$. The dominant creation and destruction channels that connect plasma species with concentrations that are most affected in case of non-equilibrium EEDF are schematically illustrated in fig. 8. Only the strongest paths have been presented here. Often indicated pathways do not add up to 100% because of the channels that could not be shown here to keep the figure readable. The loss processes in equilibrium (MB) and non-equilibrium (BE) cases are marked at the beginning of arrow and sources are marked at the end of the arrow, accompanied by percentage of contribution, for each particular species.

If one checks fig. 8 one could be tempted to assume that the presented percentage contribution change in transition from the MB to BE distributions is not large. That is only the percentage of the total contribution and in some cases these percentages do not change much even when overall rates shown in figs. 2 and 3 (and the resulting densities from fig. 6) are changed. Thus one should always bear in mind the combination of the data from figs. 3 and 4, from fig. 6 and finally shown in fig. 8.

As is expected according to the analysis in sect. 2.1, the most pronounced differences in the main chemical pathways are observed in case of electron impact processes with high energy thresholds. The electron impact excitation and ionization of helium (processes R1 and R2 with MB rate coefficients in table 2, respectively) are dominant processes for the creation of He^* and He^+ in the equilibrium case, with 100% of contribution. In the non-equilibrium case, both electron impact processes have significantly lower rate coefficients (fig. 3(a)). The electron impact excitation of He is still the main source of He^*, but with net production rate which is now four orders of magnitude lower. The He^+ ion is mainly created in the ionization of helium metastable He^* (almost 100%), in accordance with the somewhat lower energy threshold for this process [63] 4.77 eV (of course this process still bears the effect of a high threshold for excitation of the metastable level 19.8 eV). Therefore, the net production rate of this process is significantly lower due to low He^* concentration (fig. 6, BE case).

Furthermore, positive oxygen ions are linked with metastable He^* and He^+ ions through Penning ionization and charge transfer, respectively. In the equilibrium case (MB), O^+ and $O_2{}^+$ ions are created with around 60% of contribution through

$$He^* + O \rightarrow He + O^+ + e^-, \qquad k_{(5)} = 2.6 \cdot 10^{-10}\,\mathrm{cm}^3/\mathrm{s}, \tag{5}$$

$$He^* + O_2 \rightarrow He + O_2{}^+ + e^-, \qquad k_{(6)} = 2.6 \cdot 10^{-10}\,\mathrm{cm}^3/\mathrm{s}, \tag{6}$$

with additional O^+ creation through the process

$$He^+ + O_2 \rightarrow He + O + O^+, \qquad k_{(7)} = 1.07 \cdot 10^{-9}(T_g/300)^{0.5}\,\mathrm{cm}^3/\mathrm{s}, \tag{7}$$

with $\approx 25\%$ of contribution. In the non-equilibrium case Penning ionization has an appreciably lower contribution in O^+ and $O_2{}^+$ creation, around 14% for O^+ and $< 1\%$ for $O_2{}^+$, despite the fact that process (6) is still dominant in He^* destruction (contribution $> 80\%$). Also, the contribution of the dissociative charge transfer (7) is below 0.1%. The processes which now apparently dominate in the production of O^+ are electron impact ionization of excited oxygen species $O(^1S)$, $O(^1D)$ with 17% of contribution, and dissociative ionization of the ground and excited O_2 states (contribution 65%). However, the cross sections for these processes are not included in the MORGAN database [58] and their rate coefficients were taken in from paper [15], so the non-equilibrium rates could not be calculated for the production of O^+.

In essence a presentation through graphs, such as fig. 8, is difficult to understand. It refers to the situation where all concentrations are close to equilibrium. All of the initial gases maintained their original abundance and were not depleted so we needed not to recalculate the rates during the development of the plasma. From that figure one could conclude that $O_4{}^+$ is the main source of $O_2{}^+$. That is of course not correct as these reactions are just part of a loop coupling $O_2{}^+$ and $O_4{}^+$. The only channels that produce new $O_2{}^+$ are the direct electron-induced ionization of the molecular O_2 (that is not shown in the figure as it would become too complex) and Penning ionization of O_2 by the metastable helium. Having seen the dependence of both BE and MB distribution functions in the region between the ionization potential of O_2 and the threshold for He metastable and having in mind the densities of helium and oxygen one could estimate that these two channels would be of similar importance. In the initial phase of the discharge only direct ionization would be effective and later on the population of $O_4{}^+$ would develop. Only then a loop may form between $O_2{}^+$ and $O_4{}^+$ and may begin to appear as the dominant channel in production of both of these species where in essence these processes just shuffle the population from one ion to the other and back [57].

The concentrations of negative ions in fig. 6 are generally higher in the non-equilibrium case. So, the introduction of the BE EEDF leads to an increase of plasma electronegativity [8,15]. As can be seen in fig. 8, two-body and three-body attachments are important channels for the creation of O^- and $O_2{}^-$. The rate coefficients for two-body dissociative attachment to excited molecular states ($O_2(^1\Sigma)$ and $O_2(^1\Delta)$) are higher than the one for attachment to the ground state of O_2 (fig. 4(a)) in the energy interval of interest (1.8 eV–3.1 eV). So, the attachment to $O_2(^1\Sigma)$ (R14) has a similar contribution to O^- creation as attachment to O_2 (R13), despite the lower concentration of the former state. The processes R13 and R14 make 42% and 45% of contribution in the MB case, respectively. The difference between the two channels of attachment is more pronounced in the BE case, where attachment R14 contributes with more than 60%, and attachment R13 with only 14%.

The most pronounced creation process of $O_2{}^-$ is the 3-body attachment in the presence of He as the third particle, due to its high concentration. BE rate coefficients for the three-body attachment in the presence of He and O_2, normalized to the third particle concentration, have similar values as MB rates, as shown in fig. 4(b). However, the contribution of the three-body attachment with He, which in the equilibrium case is around 84%, decreases to 50.7% in the non-equilibrium case since a new creation process

$$O_3{}^- + O \rightarrow O_2 + O_2{}^-, \qquad k_{(8)} = 2.5 \cdot 10^{-10}(T_g/300)^{0.5}\,\mathrm{cm}^3/\mathrm{s}, \tag{8}$$

becomes important, with 30% contribution (not shown in fig. 8). The contribution of (8) is increased in BE case because the concentration of $O_3{}^-$ ions that is higher by one order of magnitude than in the MB case (fig. 6), where this process participates with only 3% of the contribution.

As is noted at the beginning of sect. 3, the concentration of the third group of plasma species in fig. 6 is little affected by an introduction of the non-equilibrium EEDF. In the case of the excited oxygen molecular states the BE and MB rate coefficients have similar values (figs. 3(a), (b)) and this fact explains their similar concentrations. In case of reactions where one reactant is from the group of negative ions, with an increased concentration, reaction products could be slightly increased. For example, the main process of O atom production in the BE case involves O_3^- ions and He ground state. An increase of the O_3 concentration induces doubling of O concentration. In case where both reactants are alerted, but in a different direction, the concentration of products remains the same, as in the case of H atom production in reaction of O and OH. In the third case, one of the reactants is from the group of positive ions with decreased concentration and one is not alerted, and in this case the net production rate is lower. This is the case in N atoms production through processes which involve O^+, N_2^+ and NO^+ ions. A similar conclusion holds and in the case of NO_x oxides with kinetic that is mutually strongly coupled and mainly depends on kinetics of NO^+ ions. Thus a decrease in ion concentration leads to a decrease in NO_x oxides concentrations.

An important task in modeling atmospheric pressure plasmas formed in mixtures which contain water is the determination of the production mechanisms of OH radicals, which are marked as one of the most strongly oxidative species in this type of plasmas [9]. In plasmas with water content around a part of a percent (or several thousand ppm), the process of the electron impact dissociation of water is considered as one of the dominant mechanisms of OH production [7,9]. On the other hand, our results and results [15] suggest that in mixtures with real air/nitrogen and with low water content (of the order of ppm), heavy particle collisions take a dominant role in the creation of OH radicals. This conclusion is based on the fact that nitrogen oxides NO_2 and NO_3 carry more than 90% of OH creation, in both equilibrium and non-equilibrium cases. So, the OH kinetic depends on the assumed EEDF through processes which determine NO^+ and NO_x kinetics.

4 Summary and conclusions

In this work we have presented an analysis of the influence of the non-equilibrium EEDF, taken in its most easily accessible two-term approximation form, on the chemical kinetics of the most important plasma species in atmospheric pressure He/O_2 plasmas which also contains humid air. We have determined the characteristic chemical pathways and evaluated the most important physicochemical processes in the balance of important plasma species, according to the results of the 0D global model with the electron rate coefficients based on Maxwell-Boltzmann and non-equilibrium EEDF. In general, we may conclude that the representation of electrons by the MB distribution is rather robust if not entirely accurate for processes mainly induced directly by electrons if energy losses are of the same order as the mean energy. This representation fails seriously, as expected [18], for processes with much higher thresholds than the mean energy. Such processes have much slower rates in non-equilibrium plasmas, since the non-equilibrium EEDF most frequently (but not always [19]) has a few orders of magnitude lower high-energy tail due to effect of the inelastic processes on the electron energy balance. As a result, concentrations of He^+ ions and He^* metastables generated in electron impact processes are lowered causing a change of kinetics of plasma species generated in heavy particle collisions of He_2^*, He_2^+, and of positive and negative oxygen ions. Our calculation shows that Penning ionization has a considerably lower contribution in ion creation in the non-equilibrium case. Two-body and three-body electron attachment are little affected by the transition from the MB to the BE EEDF, since these processes have very low thresholds in the region where the MB and BE EEDF have similar values. Having in mind the influence of the EEDF energy dependence on rates and therefore on kinetics of plasma itself one needs to be extra careful in deciding to which degree the profile of the plasma EEDF is really MB-like. Often, for a wide energy range an MB distribution may appear to be valid especially from the probe data but then for higher energies that are critical for ionization and excitation (to such states as He metastable) a quite different temperature is required and perhaps the two temperature MB distribution may only be an indication of the need to correct for the proper energy dependence at higher energies. One may claim that in mixtures of molecular gases with He most ionization is from the ionization of the molecular component but even then, thresholds are reasonably high to warrant an analysis as the one performed here and also the contribution of the Penning ionization may be strongly dependent on the distribution functions that are relevant in the studied plasma. Thus we have strong effects of the shape of the EEDF on He^*, He_2^*, He^+, He_2^+, O^+, and all the positive molecular ions (although to a somewhat lesser extent). In addition negative ions are also affected but in the opposite direction, the smaller positive ion densities reduce losses of negative ions. However, this is a 0D calculation and adding drift and diffusion to the electrodes may reduce the effect on negative ions.

As a special parametric study we have varied the charge density thus allowing a gradual transition from the low charge density to the high charge density limit. Thus we provide a guidance as to when the MB based rates for electrons may become an accurate option for modeling.

Finally, our results suggest that in plasmas created in mixtures containing real air with low water content (of the order of ppm), heavy particle collisions take over a dominant role in the kinetics of reactive oxygen and nitrogen species.

This work is supported by MPNTR of Serbia, projects ON171037 and III41011.

References

1. I. Adamovich, S. Baalrud, A. Bogaerts, P.J. Bruggeman, M. Cappelli, V. Colombo, U. Czarnetzki, U. Ebert, J.G. Eden, P. Favia, D.B. Graves, S. Hamaguchi, G. Hieftje, M. Hori, I.D. Kaganovich, U. Kortshagen, M.J. Kushner, N.J. Mason, S. Mazouffre, S. Mededovic Thagard, H.R. Metelmann, A. Mizuno, E. Moreau, A.B. Murphy, B.A. Niemira, G.S. Oehrlein, Z. Lj. Petrovic, L.C. Pitchford, Y.K. Pu, S. Rauf, O. Sakai, S. Samukawa, S. Starikovskaia, J. Tennyson, K. Terashima, M.M. Turner, M.C.M. van de Sanden, A. Vardelle, J. Phys. D **50**, 323001 (2017).
2. M.A. Lieberman, A.J. Lichtenberg, *Principles of Plasma Discharges and Materials Processing*, 2ed. (John Wiley & Sons, New Jersey, 2005) p. 757.
3. T. Makabe, Z. Petrović, *Plasma electronics: Applications in Microelectronic Device Fabrication* (Tayler & Francis Group, New York and London, 2006) p. 330.
4. N. Puač, Z. Lj. Petrović, G. Malović, A. Đorđević, S. Živković, Z. Giba, D. Grubišić, J. Phys. D **39**, 3514 (2006).
5. M.G. Kong, G. Kroesen, G. Morfill, T. Nosenko, T. Shimizu, J. Van Dijk, J.L. Zimmermann, New J. Phys. **11**, 115012 (2009).
6. A.N. Bhoj, M.J. Kushner, J. Phys. D **39**, 1594 (2006).
7. R. Dorai, M.J. Kushner, J. Phys. D **36**, 666 (2003).
8. D.X. Liu, M.Z. Rong, X.H. Wang, F. Iza, M.G. Kong, P. Bruggeman, Plasma Process. Polym. **7**, 846 (2010).
9. P. Bruggeman, D.C. Schram, Plasma Sources Sci. Technol. **19**, 045025 (2010).
10. D.X. Liu, P. Bruggeman, F. Iza, M.Z. Rong, M.G. Kong, Plasma Sources Sci. Technol. **19**, 025018 (2010).
11. S.A. Norberg, E. Johnsen, M.J. Kushner, Plasma Sources Sci. Technol. **24**, 035026 (2015).
12. K.R. Stalder, R.J. Vidmar, G. Nersisyan, W.G. Graham, J. Appl. Phys. **99**, 093301 (2006).
13. D.X. Liu, F. Iza, X.H. Wang, M.G. Kong, M.Z. Rong, Appl. Phys. Lett. **98**, 221501 (2011).
14. Y. Sakiyama, D.B. Graves, H.W. Chang, T. Shimizu, G.E. Morfill, J. Phys. D **45**, 425201 (2012).
15. T. Murakami, K. Niemi, T. Gans, D. O'Connell, W.G. Graham, Plasma Sources Sci. Technol. **22**, 015003 (2013).
16. P.J. Bruggeman, M.J. Kushner, B.R. Locke, J.G.E. Gardeniers, W.G. Graham, D.B. Graves, R.C.H.M. Hofman-Caris, D. Maric, J.P. Reid, E. Ceriani, D. Fernandez Rivas, J.E. Foster, S.C. Garrick, Y. Gorbanev, S. Hamaguchi, F. Iza, H. Jablonowski, E. Klimova, J. Kolb, F. Krcma, P. Lukes, Z. Machala, I. Marinov, D. Mariotti, S. Mededovic Thagard, D. Minakata, E.C. Neyts, J. Pawlat, Z. Lj. Petrovic, R. Pflieger, S. Reuter, D.C. Schram, S. Schröter, M. Shiraiwa, B. Tarabová, P.A. Tsai, J.R.R. Verlet, T. von Woedtke, K.R. Wilson, K. Yasui, G. Zvereva, Plasma Sources Sci. Technol. **25**, 053002 (2016).
17. T. Murakami, K. Niemi, T. Gans, D. O'Connell, W.G. Graham, Plasma Sources Sci. Technol. **23**, 025005 (2014).
18. Z. Lj. Petrović, M. Šuvakov, Ž. Nikitović, S. Dujko, O. Šašić, J. Jovanović, G. Malović, V. Stojanović, Plasma Sources Sci. Technol. **16**, S1 (2007).
19. Z. Lj. Petrović, S. Dujko, D. Marić, G. Malović, Ž. Nikitović, O. Šašić, J. Jovanović, V. Stojanović, M. Radmilović-Radenović, J. Phys. D **42**, 194002 (2009).
20. G.J.M. Hagelaar, L.C. Pitchford, Plasma Sources Sci. Technol. **14**, 722 (2005).
21. G.J.M. Hagelaar, Plasma Sources Sci. Technol. **25**, 015015 (2016).
22. Z. Donko, N. Dyatko, Eur. Phys. J. D **70**, 135 (2016).
23. C. Lazzaroni, P. Chabert, M.A. Lieberman, A.J. Lichtenberg, A. Leblanc, Plasma Sources Sci. Technol. **21**, 035013 (2012).
24. A. Hurlbatt, A.R. Gibson, S. Schroter, J. Bredin, A.P.S. Foote, P. Grondein, D. O'Connell, T. Gans, Plasma Process. Polym. **14**, 1600138 (2017).
25. S. Rauf, M.J. Kushner, J. Appl. Phys. **85**, 3460 (1999).
26. N. Nakano, N. Shimura, Z. Lj. Petrović, T. Makabe, Phys. Rev. E **49**, 4455 (1994).
27. T. Makabe, N. Nakano, Y. Yamaguchi, Phys. Rev. A **45**, 2520 (1992).
28. T.J. Sommerer, M.J. Kushner, J. Appl. Phys. **71**, 1654 (1992).
29. Z. Donko, P. Hartmann, K. Kutasi, Plasma Sources Sci. Technol. **15**, 178 (2006).
30. M.M. Turner, A. Derzsi, Z. Donko, D. Eremin, S.J. Kelly, T. Lafleur, T. Mussenbrock, Phys. Plasmas **20**, 013507 (2013).
31. S. Dujko, A.H. Markosyan, R.D. White, U. Ebert, J. Phys. D **46**, 475202 (2013).
32. A.H. Markosyan, J. Teunissen, S. Dujko, U. Ebert, Plasma Sources Sci. Technol. **24**, 065002 (2015).
33. J. Loureiro, C.M. Ferreira, M. Capitelli, C. Gorse, M. Cacciatore, J. Phys. D **23**, 1371 (1990).
34. M. Capitelli, *Nonequilibrium Vibrational Kinetics* (Springer-Verlag, Berlin, Heidelberg, 1986) p. 337.
35. G.I. Font, W.L. Morgan, G. Mennenga, J. Appl. Phys. **91**, 3530 (2002).
36. B. Gordiets, C.M. Ferreira, M.J. Pinheiro, A. Ricard, Plasma Sources Sci. Technol. **7**, 363 (1998).
37. T. Tochikubo, Z. Lj. Petrović, S. Kakuta, N. Nakano, T. Makabe, Jpn. J. Appl. Phys. **33**, 4271 (1994).
38. E. Gogolides, H.H. Sawin, J. Appl. Phys. **72**, 3988 (1992).
39. D.P. Lymberopoulos, D.J. Economou, J. Appl. Phys. **73**, 3668 (1993).
40. Ž. Nikitović, V. Stojanović, Z. Lj. Petrović, U. Cvelbar, M. Mozetič, EPL **9**, 55001 (2010).
41. Z. Lj. Petrović, D. Marić, M. Savić, S. Marjanović, S. Dujko, G. Malović, Plasma Process. Polym. **14**, 1600124 (2017).
42. V.A. Godyak, R.B. Piejak, B.M. Alexandrovich, Phys. Rev. Lett. **68**, 40 (1992).
43. E. Meeks, J.W. Shon, IEEE Trans. Plasma Sci. **23**, 539 (1995).
44. J.T. Gudmundsson, Plasma Sources Sci. Technol. **10**, 76 (2001).
45. S. Mukkavilli, C.K. Lee, K. Varghese, L.L. Tavlarides, IEEE Trans. Plasma Sci. **16**, 652 (1998).
46. R.J. Carman, R.P. Mildren, J. Phys. D **33**, L99 (2000).

47. K. Nam, J.P. Verboncoeur, Appl. Phys. Lett. **92**, 231502 (2008).
48. G. Park, H. Lee, G. Kim, J.K. Lee, Plasma Process. Polym. **5**, 569 (2008).
49. Y. Yang, Plasma Chem. Plasma Process. **23**, 327 (2003).
50. G.Z. Park, Y.J. Hong, H.W. Lee, J.Y. Sim, J.K. Lee, Plasma Process. Polym. **7**, 281 (2010).
51. R. Dorai, K. Hassouni, M.J. Kushner, J. Appl. Phys. **88**, 6060 (2000).
52. D.S. Stafford, M.J. Kushner, J. Appl. Phys. **96**, 2451 (2004).
53. M.M. Turner, Plasma Sources Sci. Technol. **24**, 035027 (2015).
54. J. Tennyson, S. Rahimi, C. Hill, L. Tse, A. Vibhakar, D. Akello-Egwel, D.B. Brown, A. Dzarasova, J.R. Hamilton, D. Jaksch, S. Mohr, K. Wren-Little, J. Bruckmeier, A. Agarwal, K. Bartschat, A. Bogaerts, J.P. Booth, M.J. Goeckner, K. Hassouni, Y. Itikawa, B.J. Braams, E. Krishnakumar, A. Laricchiuta, N.J. Mason, S. Pandey, Z. Lj. Petrović, Y.K. Pu, A. Ranjan, S. Rauf, J. Schulze, M.M. Turner, P. Ventzek, J.C. Whitehead, J.S. Yoon, Plasma Sources Sci. Technol. **26**, 055014 (2017).
55. N. Puač, M. Gherardi, M. Shiratani, Plasma Process. Polym. **15**, e1700174 (2018).
56. `http://www.lxcat.laplace.univ-tlse.fr`.
57. K. Niemi, J. Waskoenig, N. Sadeghi, T. Gans, D. O'Connell, Plasma Sources Sci. Technol. **20**, 055005 (2011).
58. Morgan database (2014), `www.lxcat.net`, retrieved 11 February 2014.
59. M. Capitelli, R. Celiberto, G. Colonna, F. Esposito, C. Gorse, K. Hassouni, A. Laricchiuta, S. Longo, *Fundamental Aspects of Plasma Chemical Physics Kinetics, Springer Series on Atomic, Optical, and Plasma Physics* (Springer, New York, 2016) p. 318.
60. G. Colonna, M. Capitelli, J. Phys. D **34**, 1812 (2001).
61. V. Guerra, P.A. Sa, J. Loureiro, Eur. Phys. J. Appl. Phys. **28**, 125 (2004).
62. L.D. Pietanza, G. Colonna, G. D'Ammando, A. Laricchiuta, M. Capitelli, Phys. Plasmas **23**, 013515 (2016).
63. A.J. Dixon, J. Phys. B: Atom. Mol. Phys. **9**, 15 (1976).